

# Dynamic behaviour of dagger-shaped cantilevers for atomic force microscopy

Kangzhi Shen<sup>1</sup>, Donna C Hurley<sup>2</sup> and Joseph A Turner<sup>1,3</sup>

<sup>1</sup> Department of Engineering Mechanics, Center for Materials Research and Analysis, University of Nebraska-Lincoln, Lincoln, NE 68588-0526, USA

<sup>2</sup> Materials Reliability Division, National Institute of Standards and Technology, 325 Broadway, Boulder, CO 80305-3328, USA

E-mail: jaturner@unl.edu

Received 7 June 2004, in final form 7 September 2004

Published 20 October 2004

Online at [stacks.iop.org/Nano/15/1582](http://stacks.iop.org/Nano/15/1582)

doi:10.1088/0957-4484/15/11/036

## Abstract

Experimental techniques based on the atomic force microscope (AFM) have been developed for characterizing mechanical properties at the nanoscale and applied to a variety of materials and structures. Atomic force acoustic microscopy (AFAM) is one such technique that uses spectral information of the AFM cantilever as it vibrates in contact with a sample. In this paper, the dynamic behaviour of AFM cantilevers that have a dagger shape is investigated using a power-series method. Dagger-shaped cantilevers have plan-view geometry consisting of a rectangular section at the clamped end and a triangular section at the tip. Their geometry precludes modelling using closed-form expressions. The convergence of the series is demonstrated and the convergence radius is shown to be related to the given geometry. The accuracy and efficiency of the method are investigated by comparison with finite element results for several different cases. AFAM experiments are modelled by including a linear spring at the tip that represents the contact stiffness. The technique developed is shown to be very effective for inversion of experimental frequency information into contact stiffness results for AFAM. In addition, the sensitivities of the frequencies to the contact stiffness are discussed in terms of the various geometric parameters of the problem including the slope, the ratio of the rectangular to triangular lengths and the tip location. Calculations of contact stiffness from experimental data using this model are shown to be very good in comparison with other models. It is anticipated that this approach may be useful for other cantilever geometries as well, such that AFAM accuracy may be improved.

## 1. Introduction

The dynamic behaviour of cantilever probes, including the resonant frequencies, in atomic force microscopy (AFM) has been widely used for practical estimations of material properties at the nanoscale since its invention in 1986 [1–6]. In some cases, researchers have found the dagger geometry useful for AFM measurements. However, the dynamic techniques have been limited for dagger-shaped cantilevers because of the complexity of the governing equations and the boundary

conditions. Unfortunately, closed-form solutions for the natural resonances and vibrational modes of dagger-shaped cantilevers have not been found. Thus, most investigations related to AFM analysis for related beams are based on numerical methods, such as the finite element method [6–8].

In this paper, the dynamic behaviour of a general dagger-shaped cantilever with three distinct regions, shown in figure 1, is considered. The cantilever has one region with constant cross section and two linearly varying regions. The thickness is assumed constant over the entire length. In addition, the AFM tip position is allowed to be variable such that it need not lie exactly at the end of the cantilever.

<sup>3</sup> Author to whom any correspondence should be addressed.

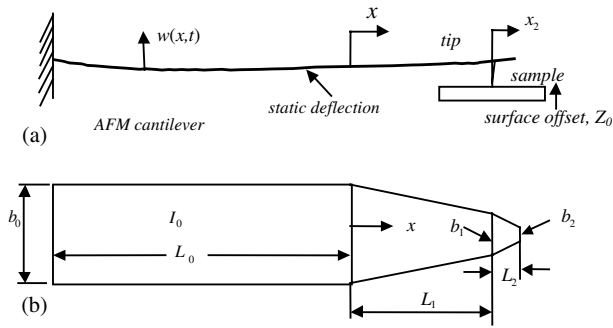


**Figure 1.** Schematic of the AFM contact problem (a) and a plan-view geometry of the dagger cantilever (b).

Because of the complexity of the governing equations of the dagger-shaped cantilever, a power series expansion is employed to determine the vibrational modes of the cantilever. The convergence of the power series is shown, and the convergence radius of the series is given. The characteristic equation is expressed as a power series by employing all of the boundary and continuity conditions. Thus, the natural frequencies of the beam are derived in a straightforward manner. The dynamic behaviour of various kinds of dagger-shaped cantilevers with different geometries and different contact positions may then be studied without difficulty.

One application of this analysis arises in atomic force acoustic microscopy (AFAM) measurements [2, 5, 6]. In this case, the measured resonant frequencies are used to determine the contact stiffness and subsequently the material properties of the sample. As shown below, numerical results indicate that the power-series solution described here is more effective for inverse analysis than the finite element method (FEM) used previously [6]. The effectiveness of the method is demonstrated by a very good agreement for the wavenumbers of the system with the results of the FEM for different geometries and different contact positions. Using the characteristic equation, the sensitivity of the wavenumbers to the contact stiffness is studied with emphasis on the effects of cantilever geometry.

Section 2 introduces the basic vibration model of the dagger-shaped cantilever. In section 3 the mode functions are derived using a power-series expansion and the convergence of the series is shown. In section 4 the characteristic equation is derived and its applications are discussed. A comparison of finite element and power-series results is given in section 5. In section 6 the influence of geometry on the sensitivity is investigated. Then, the application of the power series for estimation of material properties is studied in section 7.

## 2. Vibration model

The atomic force microscope cantilever, shown schematically in figure 1(a), is modelled here as a Euler–Bernoulli beam. The plan view of the general dagger-shaped beam considered here is shown in figure 1(b). It is clamped at one end and near the opposite end of the cantilever a tip with small radius is attached. The tip–sample contact is modelled here as a linear spring. Usually, the tip is not located exactly at the end of the cantilever. The linear boundary-value problem for this system

has different governing equations and boundary conditions for the different regions given by the left region with constant cross section, and the centre and the right regions with linearly varying cross sections. The governing equation and boundary conditions for the left region with constant cross section and length  $L_0$  are given by [9, 10]

$$EI_0 \frac{\partial^4 w_0(x, t)}{\partial x^4} + \rho A_0 \frac{\partial^2 w_0(x, t)}{\partial t^2} = 0, \quad (1)$$

$$w_0(-L_0, t) = 0, \quad \left. \frac{\partial w_0(x, t)}{\partial x} \right|_{x=-L_0} = 0.$$

The governing equation and continuity conditions for the centre region with linearly varying cross section are given by

$$EI_0 \frac{\partial^2}{\partial x^2} \left[ \left( 1 - \eta_1 \frac{x}{L_1} \right) \frac{\partial^2 w_1(x, t)}{\partial x^2} \right] + \rho A_0 \left( 1 - \eta_1 \frac{x}{L_1} \right) \frac{\partial^2 w_1(x, t)}{\partial t^2} = 0,$$

$$w_0(0^-, t) = w_1(0^+, t), \quad \frac{\partial w_0(0^-, t)}{\partial x} = \frac{\partial w_1(0^+, t)}{\partial x}, \quad (2)$$

$$\frac{\partial^2 w_0(0^-, t)}{\partial x^2} = \frac{\partial^2 w_1(0^+, t)}{\partial x^2},$$

$$\frac{\partial^3 w_0(0^-, t)}{\partial x^3} = \frac{\partial^3 w_1(0^+, t)}{\partial x^3} - \frac{\eta_1}{L_1} \frac{\partial^2 w_1(0^+, t)}{\partial x^2}.$$

Finally, if the weight of the tip is neglected, the governing equation, continuity conditions and boundary conditions for the right region are given by

$$EI_0 \frac{\partial^2}{\partial x^2} \left[ \left( 1 - \eta_2 \frac{x}{L_2} \right) \frac{\partial^2 w_2(x, t)}{\partial x^2} \right] + \rho A_0 \left( 1 - \eta_2 \frac{x}{L_2} \right) \frac{\partial^2 w_2(x, t)}{\partial t^2} = 0,$$

$$w_2(L_1^+, t) = w_1(L_1^-, t), \quad \frac{\partial w_2(L_1^+, t)}{\partial x} = \frac{\partial w_1(L_1^-, t)}{\partial x}, \quad (3)$$

$$\frac{\partial^2 w_2(L_1^+, t)}{\partial x^2} = \frac{\partial^2 w_1(L_1^-, t)}{\partial x^2},$$

$$\frac{\partial^3 w_1(L_1^-, t)}{\partial x^3} - \frac{\partial^3 w_2(L_1^+, t)}{\partial x^3} = k^* w_2(L_1^+, t) = k^* w_1(L_1^-, t),$$

$$\frac{\partial^2 w_2(L_1 + L_2, t)}{\partial x^2} = 0, \quad \frac{\partial^3 w_2(L_1 + L_2, t)}{\partial x^3} = 0.$$

In equations (1)–(3),  $\eta_1 = 1 - b_1/b_0$ ,  $\eta_2 = 1 - b_2/b_1$  define the slope factors of the cantilever width. When the slopes at both the centre part and the right part of the beam are the same, we can also employ a single slope factor  $\eta = 1 - b_2/b_0$ , where  $b_0$ ,  $b_1$  and  $b_2$  are the widths for the constant part, the tip region and the end of the cantilever, respectively. The lengths for the left, centre and right regions are  $L_0$ ,  $L_1$  and  $L_2$ , respectively.  $E$  is the Young’s modulus of the cantilever,  $I_0$  and  $A_0$  are the area moment of inertia and area of the constant cross section, respectively, and  $\rho$  is the mass density. The additional deflections about the equilibrium position are given by  $w$ , with  $w_0$ ,  $w_1$  and  $w_2$  defining the deflections for the left, centre and right regions, respectively. Here,  $k^*$  is the linear contact stiffness. It should be noted that the linear contact stiffness assumed here does not explicitly include specifics

of the tip, such as tip radius and tip shape. Although these aspects are critical to the AFM contact mechanics problem, they are beyond the scope of this work, since the focus is on the influence of the dagger-shape on the vibrational behaviour.

### 3. Mode functions

The general solution to equation (1) is found by seeking a harmonic solution  $w_0(x, t) = X(x/L_0)e^{i\omega t}$  for  $-L_0 \leq x \leq 0$ . The mode function is then given by

$$X\left(\frac{x}{L_0}\right) = A \left[ \sin kL_0 \left(\frac{x}{L_0} + 1\right) - \sinh kL_0 \left(\frac{x}{L_0} + 1\right) \right] + B \left[ \cosh kL_0 \left(\frac{x}{L_0} + 1\right) - \cos kL_0 \left(\frac{x}{L_0} + 1\right) \right], \quad (4)$$

where  $k^4 = \frac{\rho A_0}{EI_0} \omega^2$  with  $k$  as the wavenumber.

The general harmonic solution to equation (2) for the centre region of the beam with linearly varying cross section is found by the form  $w_1(x, t) = Y(x/L_1)e^{i\omega t}$  for  $0 \leq x \leq L_1$ . Substituting the harmonic solution into equation (2), a fourth-order ordinary differential equation is derived as

$$\left(1 - \eta_1 \frac{x}{L_1}\right) Y'''' - 2\eta Y''' - \gamma_1^4 \left(1 - \eta_1 \frac{x}{L_1}\right) Y = 0, \quad (5)$$

where  $\gamma_1^4 = k^4 L_1^4$ , and the primes indicate derivatives with respect to  $x/L_1$ .

A closed-form solution to equation (5) is not available. Thus, we seek a power-series solution of the form

$$Y\left(\frac{x}{L_1}\right) = \sum_{n=0}^{\infty} a_n \left(\frac{x}{L_1}\right)^n. \quad (6)$$

Substituting equation (6) into (5), the general solution is given by

$$Y\left(\frac{x}{L_1}\right) = \sum_{i=0}^3 H_i S_i \left(\frac{x}{L_1}\right), \quad (7)$$

where  $H_i, i = 0, 1, 2, 3$  are constants and

$$S_i \left(\frac{x}{L_1}\right) = \sum_{n=0}^{\infty} \xi_{in} \left(\frac{x}{L_1}\right)^n.$$

Letting  $\xi_{i(-1)} = 0$ , the recursion relation for  $\xi_{i(n+1)}$  is found to be

$$\xi_{i(n+1)} = \eta_1 \frac{n-1}{n+1} \xi_{in} + \gamma_1^4 \frac{(n-3)!}{(n+1)!} \xi_{i(n-3)} - \eta_1 \gamma_1^4 \frac{(n-3)!}{(n+1)!} \xi_{i(n-4)}, \quad n \geq 3, \quad (8)$$

where  $\xi_{in} = \delta_{in}$  when  $n \leq 3$ . The convergence radius of  $Y(x/L_1)$  is  $R_1 = 1/|\eta_1|$ . When  $\eta_1 \rightarrow 0$ , it is not difficult to show that  $Y(x/L_1) = A_1 \sin(kx/L_1) + B_1 \sinh(kx/L_1) + C_1 \cosh(kx/L_1) + D_1 \cos(kx/L_1)$ .

Similarly, the general harmonic solution to equation (3) for the right region with linearly varying cross section is found using the form  $w_2 = Z(x/L_2)e^{i\omega t}$ . Substituting the harmonic solution into equation (3), we obtain an equation similar to equation (5). Thus, the mode function is given by

$$Z\left(\frac{x_2}{L_2}\right) = \sum_{i=0}^3 J_i T_i \left(\frac{x_2}{L_2}\right), \quad 0 \leq x_2 \leq L_2, \quad (9)$$

where  $x_2 = x - L_1, J_i, i = 0, 1, 2, 3$  are constants and

$$T_i \left(\frac{x_2}{L_2}\right) = \sum_{n=0}^{\infty} \zeta_{in} \left(\frac{x_2}{L_2}\right)^n,$$

where  $\zeta_{in} = \delta_{in}$  for  $n \leq 3$ .

Letting  $\zeta_{-1}^i = 0$ , the recursion relation for  $\zeta_{i(n+1)}$  is given by

$$\zeta_{i(n+1)} = \eta_2 \frac{n-1}{n+1} \zeta_{in} + \gamma_2^4 \frac{(n-3)!}{(n+1)!} \zeta_{i(n-3)} - \eta_2 \gamma_2^4 \frac{(n-3)!}{(n+1)!} \zeta_{i(n-4)}, \quad n \geq 3, \quad (10)$$

where  $\gamma_2^4 = k^4 L_2^4$ .

When  $\eta_2 \rightarrow 0$ , it can be shown that  $Z(x/L_2) = A_2 \sin(kx/L_2) + B_2 \sinh(kx/L_2) + C_2 \cosh(kx/L_2) + D_2 \cos(kx/L_2)$ . The convergence radius of  $Z(x_2/L_2)$  is  $R_2 = 1/|\eta_2|$ . Therefore, the convergence radius of the system is  $R = \min(R_1, R_2)$ .

### 4. Characteristic equation and applications

The characteristic equation of the system governing the allowable wavenumbers (and corresponding natural frequencies) is obtained by applying the boundary and continuity conditions, giving

$$\Delta_1 \Delta_4 - \Delta_2 \Delta_3 = 0, \quad (11)$$

where

$$\begin{aligned} \Delta_1 &= \sum_{i=0}^3 S_i'''(1) J_{iA}, & \Delta_2 &= \sum_{i=0}^3 S_i'''(1) J_{iD}, \\ \Delta_3 &= \Delta_5 - \frac{L_1^3 k^*}{EI_0} J_{0A}, & \Delta_4 &= \Delta_6 - \frac{L_1^3 k^*}{EI_0} J_{0D}, \end{aligned}$$

and

$$\begin{aligned} \Delta_5 &= (1 - \eta_1) \sum_{i=0}^3 S_i'''(1) H_{iA} + 2 \left( (1 - \eta_1) \frac{\eta_2 L_1}{L_2} - \eta_1 \right) \\ &\quad \times \left(\frac{L_1}{L_2}\right)^2 J_{2A} - 6(1 - \eta_1) \left(\frac{L_1}{L_2}\right)^3 J_{3A}, \\ \Delta_6 &= (1 - \eta_1) \sum_{i=0}^3 S_i'''(1) H_{iD} + 2 \left( (1 - \eta_1) \frac{\eta_2 L_1}{L_2} - \eta_1 \right) \\ &\quad \times \left(\frac{L_1}{L_2}\right)^2 J_{2D} - 6(1 - \eta_1) \left(\frac{L_1}{L_2}\right)^3 J_{3D}, \end{aligned} \quad (12)$$

where the constants  $H_{iA}, H_{iD}, J_{iA}$  and  $J_{iD}$  ( $i = 0, 1, 2, 3$ ) are given in the appendix.

We define the effective rectangular stiffness of the cantilever as  $k_{c0} = 3EI_0/(L_0 + L_1)^3$ . Then, the stiffness of the dagger-shaped cantilever is defined as the shear load needed at the contact position for a unit displacement at the same point. This expression is given by

$$k_c = \frac{k_{c0}}{1 + \alpha}, \quad (13)$$

where

$$\begin{aligned}\alpha &= \left(\frac{L_1}{L_1+L_0}\right)^3 \left(3 \int_0^1 \frac{(1-x)^2}{(1-\eta_1 x)} dx - 1\right), \\ &= \left(\frac{L_1}{L_1+L_0}\right)^3 \left[ \frac{3}{2\eta_1^3} \left( \eta_1 \ln(1-\eta_1)^4 + 3\eta_1^2 - 2\eta_1 \right. \right. \\ &\quad \left. \left. + \eta_1^2 \ln \frac{1}{(1-\eta_1)^2} + \ln \frac{1}{(1-\eta_1)^2} \right) - 1 \right].\end{aligned}$$

If  $\eta_1 = 0$ ,  $\alpha = 0$ , then  $k_c = k_{c0}$ , and the cantilever has a constant cross section to the left of the tip. If  $\eta_1 = 1$ ,  $\alpha = \frac{1}{2} \left(\frac{L_1}{L_1+L_0}\right)^3$  and  $k_c = k_{c0} / [1 + \frac{1}{2} \left(\frac{L_1}{L_0+L_1}\right)^3]$ . In this case, the width of the cantilever at the position of the tip is zero.

By using equation (13), the characteristic equation (11) may be rewritten as

$$\Delta_1 \Delta_6 - \Delta_2 \Delta_5 = \frac{3L_1^3 k^*}{(L_0 + L_1)^3 (1 + \alpha) k_c} (\Delta_1 J_{0D} - \Delta_2 J_{0A}). \quad (14)$$

The characteristic equation (14) may be simplified for several important cases:

*Case 1.* When  $k^* = \infty$ , the contact point is a pinned connection. The characteristic equation then becomes

$$J_{0A} \Delta_4 - J_{0D} \Delta_3 = 0. \quad (15)$$

*Case 2.* For many dagger-shaped cantilevers, the tip is located very near the end of the cantilever such that  $L_2 = 0$ . The characteristic equation can then be simplified as

$$\Delta_1 \Delta_4 - \Delta_2 \Delta_3 = 0, \quad (16)$$

where

$$\begin{aligned}\Delta_1 &= \sum_{i=0}^3 S_i''(1) H_{iA}, & \Delta_2 &= \sum_{i=0}^3 S_i''(1) H_{iD}, \\ \Delta_3 &= \sum_{i=0}^3 \left( (1-\eta_1) S_i'''(1) - \frac{k^* L_1^3}{EI_0} S_i(1) \right) H_{iA}, \\ \Delta_4 &= \sum_{i=0}^3 \left( (1-\eta_1) S_i'''(1) - \frac{k^* L_1^3}{EI_0} S_i(1) \right) H_{iD}.\end{aligned} \quad (17)$$

*Case 3.* When  $\eta_1 = \eta_2 = 0$ , the cross section of the cantilever is constant. Equation (14) then is simplified as

$$\begin{aligned}2k^3 \frac{EI_0}{k^*} [1 + \cos k(L_0 + L_1 + L_2) \cosh k(L_0 + L_1 + L_2)] \\ + [\cosh k(L_0 + L_1) \sin k(L_0 + L_1) \\ - \sinh k(L_0 + L_1) \cos k(L_0 + L_1)] \\ \times (1 + \cos kL_2 \cosh kL_2) \\ - (\cosh kL_2 \sin kL_2 - \sinh kL_2 \cos kL_2) = 0.\end{aligned} \quad (18)$$

This result is the same as the exact one given elsewhere [11]. This special case shows that the power series converges to the appropriate exact solution.

The main applications of the characteristic equation in AFM can be divided into three parts. First, the resonant frequencies of the cantilever can be predicted when the geometry of the system and the contact stiffness  $k^*$  (or  $k^*/k_c$ ) are known. Second, the contact stiffness  $k^*$  (or  $k^*/k_c$ ) can be determined for a given geometry from the measured

**Table 1.** Wavenumber—contact stiffness relation using the power-series for  $\eta = 0$ .

$k^*/k_c$	$k_1 L$	$k_2 L$	$k_3 L$	$k_4 L$	$k_5 L$
0	1.875 10	4.694 09	7.854 76	10.995 5	14.137 2
0.1	1.918 91	4.696 99	7.855 38	10.995 8	14.137 3
1	2.213 50	4.723 40	7.860 97	10.997 8	14.138 2
10	3.167 65	5.001 12	7.918 96	11.018 5	14.147 9
$10^2$	3.829 81	6.404 15	8.587 42	11.255 9	14.252 3
$10^3$	3.917 04	7.007 66	10.012 0	12.859 9	15.079 5
$\infty$	3.926 60	7.068 58	10.210 2	13.351 8	16.493 4

**Table 2.** Wavenumber—contact stiffness relation using the power-series for  $\eta = 0$  and  $L_2 = 2.7 \mu\text{m}$ .

$k^*/k_c$	$k_1 L$	$k_2 L$	$k_3 L$	$k_4 L$	$k_5 L$
0.1	1.919 11	4.696 67	7.85 524	10.995 7	14.137 2
1	2.215 71	4.720 14	7.859 65	10.997 1	14.137 8
10	3.194 33	4.974 81	7.905 59	11.011 4	14.143 6
$10^2$	3.896 35	6.452 98	8.501 09	11.181 5	14.207 1
$10^3$	3.986 00	7.130 76	10.178 7	12.977 5	15.342 8
$\infty$	3.995 70	7.192 75	10.389 0	13.584 7	16.779 7

resonant frequencies. Third, the characteristic equation can be employed to design the optimum geometry of the cantilever with the largest sensitivity to changes in contact stiffness. These applications are discussed in sections 6 and 7. In the following section, the power-series method is compared with a finite element solution.

## 5. Comparison of the FEM and power series

Although the convergence of the power series has been shown, its effectiveness still needs to be tested. Therefore, a comparison of the power series solution with the FEM and the exact solution is necessary. The power series converges very quickly for small  $\eta$ . When  $\eta = 0$ , by employing 22 terms, we can obtain the exact wavenumbers for different values of contact stiffness. With an increase of  $\eta$ , more terms are needed. When  $\eta \rightarrow 1$ , 100 terms are needed for an uncertainty of 0.2%. To get even more accurate results, 1400 terms are used for the computation in the power series, and 200 elements are employed in the FEM. Details of the FEM are given elsewhere [6].

First, we consider a rectangular cantilever ( $\eta_1 = \eta_2 = \eta = 0$ ) for which  $L_0 = 102 \mu\text{m}$ ,  $L_1 = 54 \mu\text{m}$ ,  $L_2 = 0$ . The results obtained by the power series, shown in table 1, are identical to the exact results [11] for all values of  $k^*/k_c$  to six significant digits.

Next, a rectangular cantilever with three regions is considered to verify the effectiveness of the power series proposed. Thus, we let  $\eta_1 = \eta_2 = \eta = 0$ ,  $L_0 = 102 \mu\text{m}$ ,  $L_1 = 51.3 \mu\text{m}$ ,  $L_2 = 2.7 \mu\text{m}$ . In the computation, 22 terms are used in the power series. The results shown in table 2 are also identical with the exact ones [11] to six significant digits.

Next, a typical dagger-shaped cantilever with the contact at one end of the cantilever is tested. To avoid the singularity associated with the zero stiffness of the cantilever at the contact, we choose  $\eta = 0.99$  and  $L_0 = 102 \mu\text{m}$ ,  $L_1 = 54 \mu\text{m}$ ,  $L_2 = 0$ . The results are shown in table 3. The maximum difference relative to the FEM results is 0.0011%.

**Table 3.** Comparison of wavenumbers calculated using the power-series (PS) and the FEM for  $\eta = 0.99$ ,  $L_0 = 102 \mu\text{m}$ ,  $L_1 = 54 \mu\text{m}$  and  $L_2 = 0$ .

	$k^*/k_c$	$k_1L$	$k_2L$	$k_3L$	$k_4L$	$k_5L$
PS	0	2.21795	5.30822	8.56923	11.70539	14.8471
FEM		2.21792	5.30820	8.56918	11.70530	14.8470
PS	10	3.42327	5.88651	8.84004	11.85827	14.9415
FEM		3.42341	5.88665	8.84009	11.85824	14.9414
PS	$10^2$	3.83340	6.76213	9.74722	12.66727	15.5845
FEM		3.83342	6.76218	9.74732	12.66739	15.5846
PS	$\infty$	3.89494	6.98494	10.1678	13.33264	16.4759
FEM		3.89493	6.98492	10.1678	13.33259	16.4759

**Table 4.** Comparison of the wavenumber calculated using the power-series and the FEM for  $\eta = 0.99$ ,  $L_0 = 102 \mu\text{m}$ ,  $L_1 = 50 \mu\text{m}$  and  $L_2 = 4 \mu\text{m}$ .

	$k^*/k_c$	$k_1L$	$k_2L$	$k_3L$	$k_4L$	$k_5L$
PS	10	3.48275	5.86936	8.78037	11.7783	14.8458
FEM		3.48295	5.87511	8.79597	11.8086	14.8930
PS	$10^2$	3.94140	6.91779	9.86326	12.6602	15.4254
FEM		3.94171	6.91950	9.87165	12.6909	15.4919
PS	$10^3$	4.00277	7.16589	10.3906	13.5864	16.7335
FEM		4.00286	7.16628	10.3914	13.5879	16.7369
PS	$\infty$	4.00975	7.19469	10.4528	13.7022	16.9283
FEM		4.00976	7.19474	10.4530	13.7028	16.9297

Finally, a general dagger-shaped cantilever is considered. The contact is assumed to be close to the end of the cantilever. Letting  $\eta_1 = 0.916667$ ,  $\eta_2 = 0.44898$ , ( $\eta = 0.99$ ),  $L_0 = 102 \mu\text{m}$ ,  $L_1 = 50 \mu\text{m}$ ,  $L_2 = 4 \mu\text{m}$ . We use 1400 terms in the power series to obtain a more accurate result. The results are shown in the table 4. The maximum error is 0.097%.

These examples show that the results by the power series method are very close to those obtained from the finite element method with an error sufficiently small for practical implementation.

## 6. Influence of geometry on sensitivity

### 6.1. Sensitivity of the wavenumber to contact stiffness

For the AFAM technique, it is important to know how the frequencies vary with the contact stiffness. Thus, the concept of sensitivity was introduced [12]. To determine the sensitivity of the system to changes in the contact stiffness, we define the sensitivity as the change in the flexural wavenumber  $kL$  to the contact stiffness [12]. Letting  $p = k^*/k_c$ , then equation (11) becomes

$$\frac{\delta(kL)}{\delta p} = -L \frac{\Delta_1 \Delta_{4,p} - \Delta_{3,p} \Delta_2}{\Delta_{1,k} \Delta_4 + \Delta_{4,k} \Delta_1 - \Delta_{2,k} \Delta_3 - \Delta_{3,k} \Delta_2}, \quad (19)$$

where  $\Delta_{i,v} = \frac{\partial \Delta_i}{\partial v}$ ,  $i = 1, 2, 3, 4$  and  $v = p, k$ .

Since  $k^4 = \frac{\rho A_0}{E I_0} \omega^2$ , we can define the dimensionless frequency as  $\tilde{\omega} = (kL)^2$ . Therefore, the sensitivity of frequency in dimensionless form can be expressed as

$$s = \frac{\delta \tilde{\omega}}{\delta p} = -2kL^2 \frac{\Delta_1 \Delta_{4,p} - \Delta_{3,p} \Delta_2}{\Delta_{1,k} \Delta_4 + \Delta_{4,k} \Delta_1 - \Delta_{2,k} \Delta_3 - \Delta_{3,k} \Delta_2}, \quad (20)$$

where

$$\Delta_{1,k} = \sum_{i=0}^3 (H_{iA,k} S''_i(1) + H_{iA} S''_{i,k}(1)),$$

$$\Delta_{2,k} = \sum_{i=0}^3 (H_{iD,k} S''_i(1) + H_{iD} S''_{i,k}(1)),$$

$$\Delta_{3,k} = \sum_{i=0}^3 \left( (1 - \eta_1) S'''_i(1) - \frac{k^* L_1^3}{E I_0} S_i(1) \right) H_{iA,k} + \sum_{i=0}^3 \left( (1 - \eta_1) S'''_{i,k}(1) - \frac{k^* L_1^3}{E I_0} S_{i,k}(1) \right) H_{iA},$$

$$\Delta_{4,k} = \sum_{i=0}^3 \left( (1 - \eta_1) S'''_i(1) - \frac{k^* L_1^3}{E I_0} S_i(1) \right) H_{iD,k} \quad (21)$$

$$+ \sum_{i=0}^3 \left( (1 - \eta_1) S'''_{i,k}(1) - \frac{k^* L_1^3}{E I_0} S_{i,k}(1) \right) H_{iD},$$

$$\Delta_{3,p} = -3 \left( \frac{L_1}{L} \right)^3 \sum_{i=0}^3 S_i(1) H_{iA},$$

and

$$\Delta_{4,p} = -3 \left( \frac{L_1}{L} \right)^3 \sum_{i=0}^3 S_i(1) H_{iD},$$

where

$$H_{ji,k} = \frac{\partial H_{ji}}{\partial k}, \quad S''_{i,k} = \frac{\partial S''_i}{\partial k},$$

$$S'''_{i,k} = \frac{\partial S'''_i}{\partial k}, \quad i = A, D; \quad j = 0, 1, 2, 3.$$

The sensitivity of the first four modes is shown in figures 2–4. For the three different types of cantilever geometries considered, the dimensionless frequencies as a whole become smaller with the increase of the slope factor  $\eta$ . When  $\eta = 0$ , that is, the cantilever has a constant cross section, the sensitivities of the first four frequencies reach a maximum. With the increase of the slope factor  $\eta$ , the sensitivities of the first four frequencies decrease compared with that at  $\eta = 0$ . At  $\eta = 1^-$ , the sensitivities arrive at a minimum.

When  $\eta = 0$ , the cantilever is rectangular, with the sensitivity shown in figure 2. Although the sensitivities decrease as a whole with the increase of contact stiffness, the sensitivities of the second and third frequencies increase slightly and then decrease quickly. When  $k^*/k_c < 10.08$ , the first frequency is more sensitive than the second and third ones. When  $k^*/k_c \geq 10.08$ , the second frequency becomes more sensitive than the first one. When  $k^*/k_c \geq 25.38$ , the third frequency is more sensitive than the first one.

However, when  $\eta$  is close to 1, as shown in figure 2, such as  $\eta = 0.99$ , the sensitivities never increase with an increase of contact stiffness for all the frequencies. Instead, they drop quickly with an increase of the contact stiffness. When  $k^*/k_c < 15.129$ , the first frequency is more sensitive than the second and third ones. When  $k^*/k_c \geq 15.129$ , the second frequency becomes more sensitive than the first one. When  $k^*/k_c \geq 29.06$ , the third frequency is more sensitive than the first one. Finally, when  $k^*/k_c \geq 50.640$ , the fourth frequency is more sensitive than the first one. If this contact

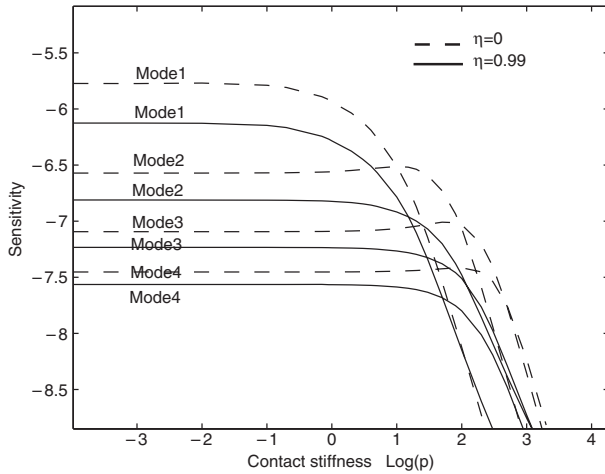


**Figure 2.** Sensitivity of the frequencies to the contact stiffness for different slope factors.

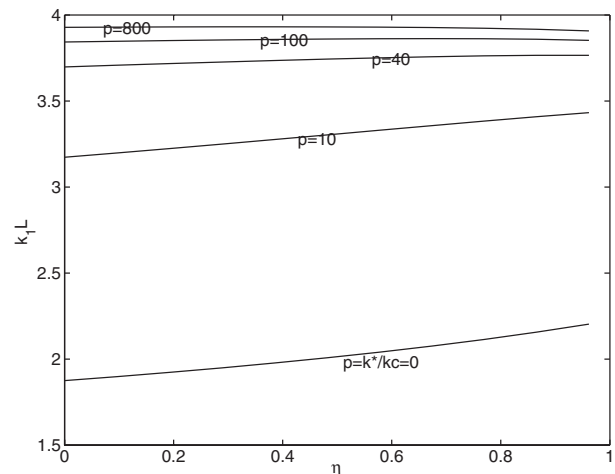


**Figure 5.** Relation between the first wavenumber and slope factor for different contact stiffnesses.

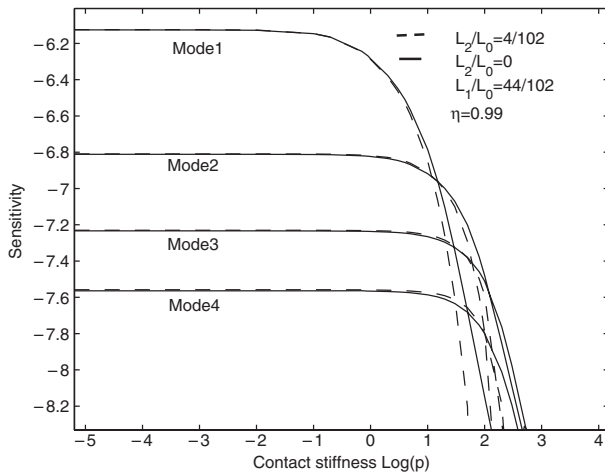


**Figure 3.** Sensitivity–contact stiffness relation for different values of  $L_2$ .

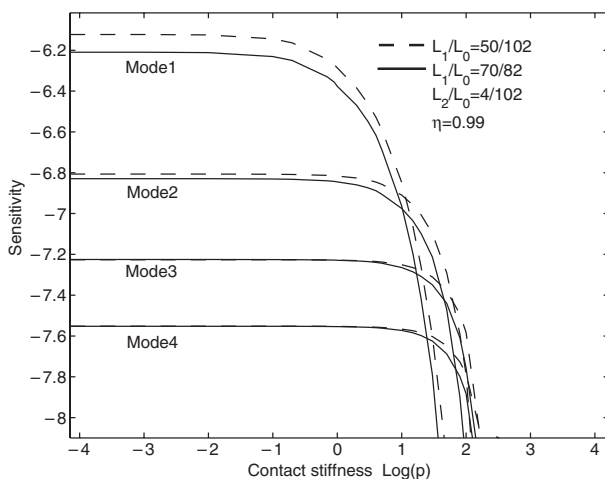


**Figure 4.** Sensitivity for different ratios  $L_0/L_1$  for  $\eta = 0.99$ .

stiffness controlling the order of the sensitivity is called the critical contact stiffness, it becomes larger with the increase of the slope factor, and the sensitivity becomes more important

because the varying ranges of the contact stiffness become larger compared with that of a rectangular one.

Next, the behaviour of the sensitivity for different contact positions is studied. With the slope factor of  $\eta = 0.99$ , the sensitivity of the first four modes for both  $L_2 = 0$  and  $L_2 = 4 \mu\text{m}$  is shown in figure 3. Although the sensitivity of the different modes is almost the same for different values of  $L_2$  at small contact stiffness, it decreases more quickly with increasing  $L_2$ . The critical contact stiffness decreases with a small increase in the length  $L_2$ .

Finally, we investigate the influence of the ratio  $L_1/L_0$  on the sensitivity, which is shown in figure 4. The sensitivity for all the modes increases with a decrease of  $L_1/L_0$ . The critical contact stiffness increases with the decrease of  $L_1/L_0$ .

### 6.2. Relation between wavenumber and slope factor

For small contact stiffness  $k^*/k_c$ , the frequencies or wavenumbers shown in figures 5–7 were observed to increase with the increase of the slope factor  $\eta$ . However, when the contact stiffness is greater than some critical value, the wavenumbers are seen to have a peak at a value of  $\eta < 1$ . That is, they do not increase monotonically with an increase of slope factor  $\eta$  for a given value of contact stiffness. They initially increase until reaching a maximum, then decrease, approaching the results for  $\eta = 1$ . This interesting behaviour was observed for the first several wavenumbers.

In order to clarify this result, the values of  $p$  and  $\eta$  that correspond to the maximum wavenumber are plotted in figure 8 for the first three modes using the same geometry as in figures 5–7. For a given contact stiffness  $k^*/k_c$  these maxima do not always occur as  $\eta \rightarrow 1$ , but change with  $k^*/k_c$ . For a fixed  $k^*/k_c$ , the maximum wavenumbers occur at a critical slope factor called  $\eta_{cr}$ , which has the value of 1 when the contact stiffness is less than a critical value. Then it decreases with the increase of the contact stiffness. For example, when  $p \leq 40$ , the first wavenumber always has its maximum for the rectangular case ( $\eta \rightarrow 1$ ). However, with increased contact stiffness,  $\eta_{cr}$  becomes smaller, as shown in figure 8. For the second and third wavenumbers, the situation is similar, but the minimum contact stiffness for this wavenumber is larger.

**Table 5.** Comparison of results from atomic force acoustic microscopy (AFAM) measurements using the power-series (PS) and the FEM.

Model	PS			FEM		
	Reference	Glass	Si	Average	Glass	Si
$M(n = 1)$ (GPa)	$83 \pm 2$	$131 \pm 5$	$107 \pm 4$	$86 \pm 2$	$136 \pm 5$	$109 \pm 5$
$M(n = \frac{3}{2})$ (GPa)	$84 \pm 2$	$120 \pm 6$	$102 \pm 5$	$87 \pm 4$	$125 \pm 6$	$105 \pm 6$

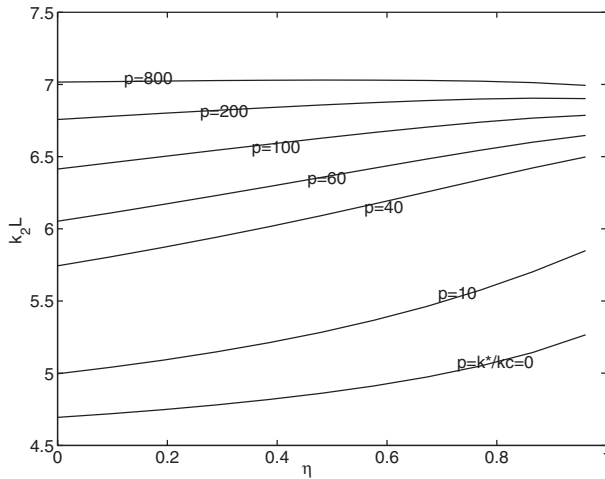


**Figure 6.** Relation between the second wavenumber and slope factor for different contact stiffnesses.

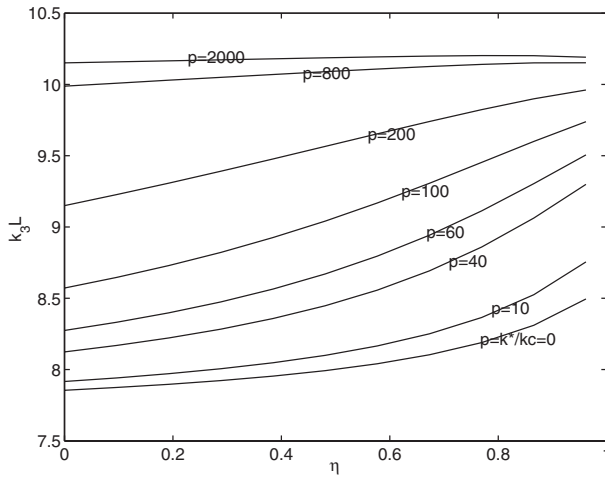


**Figure 7.** Relation between the third wavenumber and slope factor for different contact stiffnesses.

### 7. Application of power series for determining material properties

The accuracy of the power series was shown in table 5 with a good agreement with finite element results. Most importantly, the power-series method provides a direct inversion of frequency data to contact stiffness without iteration. The power series is now applied to estimate material properties of a thin film of niobium (Nb) by AFAM.

AFAM is usually employed to determine the material properties at the nanoscale by measuring the resonant frequencies of a cantilever contacting at the end with the material. Using the measured resonant frequencies under both free and contact conditions, information for both the elastic

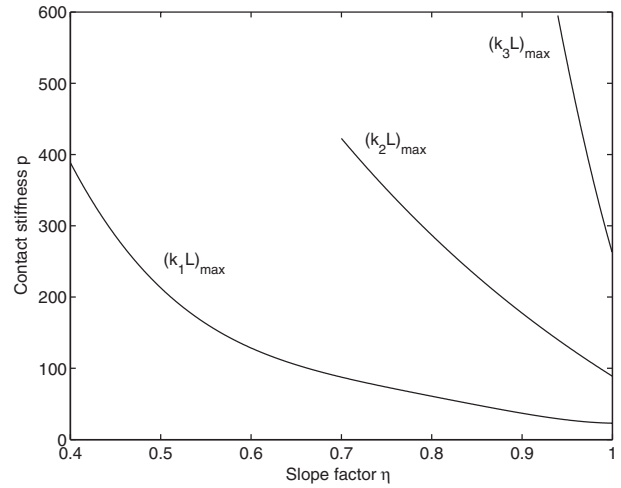


**Figure 8.** Dependence of the maximum wavenumber on contact stiffness and slope factor for the first three modes.

properties of the cantilever and the sample can be extracted directly from the characteristic equation,

$$k^* = \frac{(L_0 + L_1)^3 (1 + \alpha) k_c}{3L_1^3 (\Delta_1 J_{0D} - \Delta_2 J_{0A})} (\Delta_1 \Delta_6 - \Delta_2 \Delta_5). \quad (22)$$

A reference material is usually employed in the experiment to eliminate experimental uncertainties [2, 6]. These experiments have shown that the elastic properties of the reference sample, namely its indentation modulus  $M$ , should be similar to that of the test material. For an isotropic material,  $M$  is related to Young's modulus  $E$  and Poisson's ratio  $\nu$  by  $M = E / (1 - \nu^2)$ . In this experiment, the first reference material is a (001) single-crystal silicon (Si) wafer with indentation modulus  $M_{Si} = 161$  GPa. The second one is a borosilicate crown glass disk with indentation modulus  $M_{gl} = 85 \pm 3$  GPa [6].

The computation for the indentation modulus of the test materials are based on the following equations [5]:

$$E_{test}^* = E_{ref}^* \left( \frac{k_{test}^*}{k_{ref}^*} \right)^n, \quad (23)$$

$$\frac{1}{E_{test}^*} = \frac{1}{M_{tip}} + \frac{1}{M_{test}}, \quad (24)$$

where  $n$  is the parameter of the contact model. For Hertzian contact  $n = 1.5$ , and for flat-punch contact  $n = 1$ .

To determine the indentation modulus of a Nb film sample from the resonant frequency measured previously, we use both the power-series and finite element methods for Hertzian contact ( $n = 1.5$ ) and flat-punch contact ( $n = 1$ ), respectively. The results are shown in table 5. It can be seen that the indentation modulus using the power series approach is slightly

lower than that obtained by the FEM. The maximum difference is 4%. However, it is still very close to that obtained by the finite element method. Therefore, the power series can be employed in the estimation of material properties with an error that is sufficiently small. Most importantly, the results are obtained without iteration, as is necessary with the FEM [6].

## 8. Summary

In this paper, a power-series approach has been presented for studying the dynamics of AFM cantilevers. The power series can be effectively employed in the computation for the dynamic analysis of any kind of dagger-shaped cantilever with different slope factors. The computation error is acceptably small with the error controlled by the number of terms used in the expansion. It was shown that fewer terms are needed when the slope factor of the width is small.

For the dagger-shaped cantilever, the sensitivities of all the frequencies or wavenumbers to the contact stiffness change with the slope factor. In general, the higher the slope, the lower the sensitivity. Low-order frequencies are more sensitive to the small contact stiffness. With the increase of the contact stiffness until critical values, the sensitivities of different frequencies will change.

The example results presented here represent only a few of the many applications of the power-series method. The ability of this method for direct inversion of resonant frequency measurements into contact stiffness values is clearly a major advance over other methods, such as the finite element method, developed for AFM beams with non-uniform cross sections. The development of this general solution will create new opportunities for AFAM experiments involving a greater variety of cantilevers beyond those (rectangular) currently used for AFAM. The benefits to the greater material science and engineering research community are expected to be substantial.

## Acknowledgments

This work was sponsored by the US Air Force Office of Scientific Research (Grant No. F49620-99-1-0254) and the National Science Foundation (Grant Nos. DMI-0210850, INT-0089548). Support of the Center for Electro-Optics at the University of Nebraska-Lincoln is also gratefully acknowledged.

## Appendix

To simplify equations (13), the following notation is used.

$$\begin{aligned} H_{0A} &= \sin kL_0 - \sinh kL_0, \\ H_{0D} &= \cosh kL_0 - \cos kL_0, \\ H_{1A} &= kL_1(\cos kL_0 - \cosh kL_0), \\ H_{1D} &= kL_1(\sinh kL_0 + \sin kL_0), \\ H_{2A} &= -\frac{(kL_1)^2}{2}(\sin kL_0 + \sinh kL_0), \\ H_{2D} &= \frac{(kL_1)^2}{2}(\cosh kL_0 + \cos kL_0), \end{aligned}$$

$$\begin{aligned} H_{3A} &= -\frac{(kL_1)^3}{6}(\cos kL_0 + \cosh kL_0) \\ &\quad + \eta_1 \frac{(kL_1)^2}{6}(\sin kL_0 + \sinh kL_0), \\ H_{3D} &= \frac{(kL_1)^3}{6}(\sin kL_0 - \sinh kL_0) \\ &\quad + \eta_1 \frac{(kL_1)^2}{6}(\cosh kL_0 + \cos kL_0), \end{aligned} \quad (\text{A.1})$$

$$\begin{aligned} J_{0A} &= \sum_{i=0}^3 H_{iA} S_i(1), & J_{0D} &= \sum_{i=0}^3 H_{iD} S_i(1), \\ J_{1A} &= \frac{L_2}{L_1} \sum_{i=0}^3 H_{iA} S'_i(1), & J_{1D} &= \frac{L_2}{L_1} \sum_{i=0}^3 H_{iD} S'_i(1), \\ J_{2A} &= \frac{1}{2} \left( \frac{L_2}{L_1} \right)^2 \sum_{i=0}^3 H_{iA} S''_i(1), \\ J_{2D} &= \frac{1}{2} \left( \frac{L_2}{L_1} \right)^2 \sum_{i=0}^3 H_{iD} S''_i(1), \\ J_{3A} &= -\frac{1}{K''_3(1)} \sum_{i=0}^2 J_{iA} T''_i(1), & \text{and} \\ J_{3D} &= -\frac{1}{K''_3(1)} \sum_{i=0}^2 J_{iD} T''_i(1). \end{aligned}$$

## References

- [1] de Water W V and Molenaar J 2000 Dynamics of vibrating atomic force microscopy *Nanotechnology* **11** 192–9
- [2] Rabe U, Amelio S, Kester E, Scherer V, Hirsekorn S and Arnold W 2000 Quantitative determination of contact stiffness using atomic force acoustic microscopy *Ultrasonics* **38** 430–7
- [3] Yamanaka K, Maruyama Y, Tsuji T and Nakamoto K 2001 Resonance frequency and  $Q$  factor mapping by ultrasonic atomic force microscopy *Appl. Phys. Lett.* **78** 1939–41
- [4] Dupas E, Gremaud G, Kulik A and Loubet J-L 2001 High-frequency mechanical spectroscopy with an atomic force microscope *Rev. Sci. Instrum.* **72** 3891–7
- [5] Rabe U, Amelio S, Kopycinska M, Hirsekorn S, Kempf M, Göken M and Arnold W 2002 Imaging and measurement of local mechanical material properties by atomic force acoustic microscopy *Surf. Interface Anal.* **33** 65–70
- [6] Hurley D C, Shen K, Jennett N M and Turner J A 2003 Atomic force acoustic microscopy methods to determine thin-film elastic properties *J. Appl. Phys.* **94** 2347–54
- [7] Stark R W, Drobek T and Heckl W M 2001 Thermomechanical noise of a free v-shaped cantilever for atomic-force microscopy *Ultramicroscopy* **86** 207–15
- [8] Sader J E 2002 Surface stress induced deflections of cantilever plates with applications to the atomic force microscope: V-shaped plates *J. Appl. Phys.* **91** 9354–61
- [9] Meirovich L 1986 *Elements of Vibration Analysis* (New York: McGraw-Hill)
- [10] Rao J S 1992 *Advanced Theory of Vibration* (New York: Wiley)
- [11] Rabe U, Janser K and Arnold W 1996 Vibrations of free and surface-coupled atomic force microscope cantilevers: theory and experiment *Rev. Sci. Instrum.* **67** 3281–93
- [12] Turner J A and Wiehn J S 2001 Sensitivity of flexural and torsional vibration modes of atomic force microscope cantilevers to surface stiffness variations *Nanotechnology* **12** 322–30